Polymer 52 (2011) 6117–6125

Contents lists available at SciVerse ScienceDirect

Polymer

journal homepage: www.elsevier.com/locate/polymer

Physical aging of layered glassy polymer films *via* gas permeability tracking

Thomas M. Murphy, D.S. Langhe, M. Ponting, E. Baer, B.D. Freeman, D.R. Paul*

Department of Chemical Engineering, The University of Texas at Austin, Austin, TX 78712, United States

ARTICLE INFO

Article history:
Received 26 August 2011
Received in revised form
28 October 2011
Accepted 30 October 2011
Available online 4 November 2011

Keywords:
Physical aging
Gas permeability
Confinement

ABSTRACT

The physical aging of polymers in confined environments has been an area of intensive study in recent times. The rate of physical aging in thin films of many polymers used in gas separation membranes is dependent on film thickness and accelerated relative to bulk. In this study, the physical aging of polymer films with alternating glassy polysulfone and rubbery polyolefin layers was monitored by measuring the gas permeability of O_2 and N_2 as a function of aging time at 35 °C. The alternating layer structures were formed by a melt co-extrusion process. The polysulfone layers have thicknesses ranging from 185 to 400 nm, and the overall thicknesses of the films are on the order of 80–120 μm. The aging of free-standing thin films of polysulfone is rapid and exhibits clear thickness dependence, whereas the aging of multilayered films was observed to be similar to bulk and showed no dependence on layer thickness. At 1000 h of aging time, a 400 nm freestanding PSF film decreased in O_2 permeability by 35%, whereas on average the bulk and multilayered films only experienced a decline of 10–15%. A slight increase in O_2/N_2 selectivity for the multilayered films was observed over the course of aging.

1. Introduction

"Physical aging" is a term referring to changes in the properties of a non-equilibrium glassy material as it approaches equilibrium *via* structural relaxation [1]. Physical aging below the glass transition temperature (T_g) is a characteristic feature of all amorphous materials, including polymer glasses [2,3]. In general, physical aging causes a gradual decrease in sample volume (densification), which leads to increased brittleness, decreased gas permeability, decreased enthalpy, increased refractive index, and changes in many other properties [2,3]. Fig. 1 is a schematic depiction of the physical aging process for a glass-forming polymer. Holding the glass at an aging temperature of T_a allows it to approach equilibrium as the excess volume that results from glass formation is gradually lost (*i.e.*, the driving force for physical aging is continuously eroded). Physical aging is distinct from weathering, thermal degradation, oxidation, and other such time-dependent phenomena because it is completely reversible and involves no changes in chemical structure [2]. The vast array of properties that change during physical aging allows a variety of experimental techniques to be used in tracking the aging process. Historically, some of the most common ways of studying physical aging include dilatometry, creep testing, and differential scanning calorimetry (DSC); more recently, methods such as gas permeability [4–21], fluorescence spectroscopy [22–30], and ellipsometry [8,9,13,14,31–35] have gained popularity as tools for tracking aging, especially for thin polymer films. Recent observations suggest that the glass transition temperature and physical aging can be strongly dependent on both sample size and interfacial interactions between the polymer and supporting substrate [6,20,22,24,25,33,36–39]. In general, attractive polymer-substrate interactions tend to increase the T_g of confined polymers, while free surfaces and neutral or repulsive polymer-substrate interactions tend to decrease T_g in confined systems [40].

Kawana and Jones studied the physical aging of polystyrene (PS) films *via* ellipsometry by measuring the overshoot in thermal expansivity versus temperature [33]. The characteristic temperature of the relaxation peak was independent of film thickness, but the peak intensity was inversely proportional to film thickness. They also observed that physical aging occurred in 18 nm films but could not be detected in 10 nm films. Their findings were attributed to the existence of a liquid-like surface layer on the order of 10 nm. Ellison et al. [22] used fluorescence spectroscopy to study the aging behavior of thin films of poly(isobutyl methacrylate) supported on fused quartz and found no noticeable dependence of aging rate on film thickness. The lack of thickness dependence was attributed to a possible balance between the competing effects of T_g reduction and proportionately greater polymer-substrate interaction in the thinner films. A study by Priestley et al. [24] using fluorescence observed physical aging 7 K above the bulk T_g for a chromophore-

* Corresponding author. Tel.: +1 512 471 5392; fax: +1 512 471 0542.
E-mail address: drp@che.utexas.edu (D.R. Paul).

0032-3861/$ – see front matter © 2011 Elsevier Ltd. All rights reserved.
doi:10.1016/j.polymer.2011.10.061

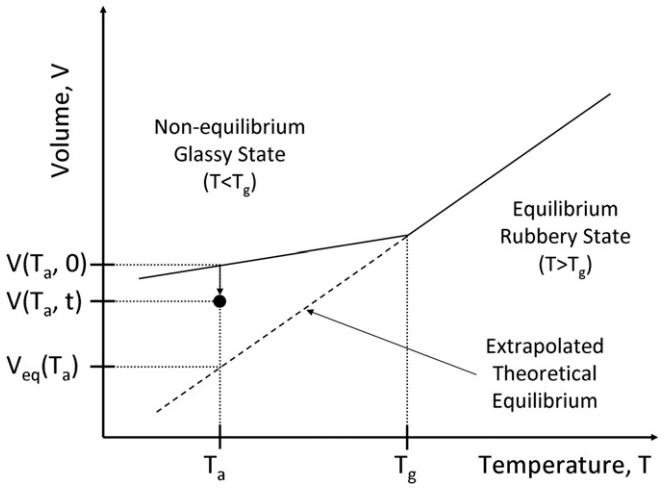

Fig. 1. Schematic state diagram for a glass-forming polymer as it undergoes physical aging.

labeled 20 nm PMMA film on a silica substrate, yet no aging was observed for a 500 nm PMMA film aged at the same temperature. The 500 nm film exhibited an increase in aging rate with decreasing aging temperature, while the 20 nm film exhibited a decreasing aging rate with decreasing aging temperature; additionally, the absolute magnitude of the aging rate in the 20 nm film was much lower than in the 500 nm film at all temperatures considered. The reduced aging rate in the ultrathin films was attributed to the attractive polymer-substrate interactions (which increase T_g and become proportionately greater as a film is made thinner), and it was suggested that the increase in aging rate with increasing temperature could be due to thermal energy overcoming some of these interactions and thereby enhancing the structural relaxation in the ultrathin sample at elevated temperatures. Later work by Priestley et al. [25] on supported PMMA films revealed a distribution of aging rates across the thickness of the film, with virtually no relaxation near the PMMA-substrate interface, bulk-like aging in the interior of the film, and a 50% decrease in aging rate at the free surface of the film. The change in relaxation rates was found to propagate over 100 nm into the film, a length scale that is greater than that over which T_g is altered by surfaces and interfacial interactions. Koh and Simon [41] used DSC to study stacked ultrathin PS films and observed a decreased and broadened T_g. In their studies, the aging of bulk and ultrathin films was similar when aged at an equivalent distance from T_g; however, when aged at a given temperature, the ultrathin films, which have a reduced T_g, require a shorter time to reach equilibrium (indicative of accelerated aging). Interestingly, when aged at the same temperature, the aging rate in the ultrathin films is less than that of bulk films due to the reduced T_g and reduced driving force for aging; thus, for aging in the near-T_g regime, the aging rate is not always the best indicator of whether or not aging is accelerated. Accelerated aging in the near-T_g regime was also observed by Boucher et al. [42], who studied the physical aging and glass transition of PS/gold nanocomposites by DSC. When aged at the same temperature, samples with greater amounts of gold nanoparticles (*i.e.*, a greater degree of confinement) reached equilibrium faster than a bulk PS sample. The finding that a decreased amount of time is required for PS/gold nanocomposite samples to reach equilibrium is similar to the observation of Koh and Simon discussed previously.

The consensus among researchers using gas permeability to track physical aging is that aging in unsupported thin films is thickness-dependent and accelerated relative to bulk [4–11,16–20]. Huang et al. studied polysulfone (PSF), Matrimid, and poly(2,6-dimethyl-1,4-phenylene oxide) films as thin as 400 nm and observed accelerated aging with decreasing film thickness, despite the fact that at these thicknesses the T_g is unchanged from the bulk value [6,8–11,32]. Rowe et al. [20] extended studies of PSF and Matrimid to films as thin as 18 nm and found that rapid aging persisted in even the thinnest films. As film thickness was decreased, the initial permeability values were lower and the initial selectivities were higher. These findings were attributed to rapid aging that occurred during the first hour of aging time (which is experimentally inaccessible using these techniques). Rapid aging during the first hour (and perhaps rapid structural relaxation that occurs during cooling to the aging temperature from above T_g) also resulted in slightly lower aging rates for the thinnest films when compared to the thicker films studied. The observations were found to be consistent with the concepts of enhanced mobility at the film surface and reduced T_g [20]. In another study, Rowe et al. [37] used variable energy positron annihilation lifetime spectroscopy (PALS) to study aging in PSF films of roughly 450 nm. The data suggested that the near-surface regions of the film contained smaller free volume elements than the film interior, a result that was attributed to enhanced mobility at the surface allowing the local polymer chains to reach a lower free volume state more rapidly. The 450 nm PSF film was found to undergo a more rapid decline in ortho-positronium lifetime than bulk, indicative of accelerated physical aging.

Without question, the topic of physical aging in confinement is a rich field of study with many questions yet to be fully answered. Multilayer co-extrusion enables the production of novel confined polymer systems whose aging behavior has not yet been explored. In this study, the gas permeability of multilayered films containing PSF was measured over time and compared against aging data for bulk and thin films. In doing so, a direct comparison is made between the behavior of thin layers with no free surfaces and that of thin, freestanding films with free surfaces.

2. Experimental

2.1. Materials

UDEL P-3700 Polysulfone (PSF) from Solvay Advanced Polymers was the primary material of interest in this study. PSF is an important material in the gas separation membrane industry, and the aging behavior of thin, freestanding films of PSF *via* gas permeability tracking has been well-characterized [6–11,16–20,37]. At the aging temperature used in this study, PSF is deep in the glassy state ($T_g \sim 185$ °C, $T_g - T_a \sim 150$ °C). Two materials supplied by Dow Chemical Co. were also used in this project: an ethylene-1-octene copolymer, Engage 8100 (EO), and an olefin block copolymer, Infuse 9007 (OBC). At the temperatures used for aging and permeability measurement in this study (35 °C), both of these materials are well above their T_gs (−52 °C and −60 °C for EO and OBC, respectively), so they do not undergo physical aging. If multilayered films were to be made with two polymers that are in the glassy state at the chosen aging temperature, the fact that both materials are aging would convolute the study and make it nearly impossible to isolate the effects of aging on either material individually. Table 1 provides a list of the materials used in this study and some of their relevant properties. EO and OBC were chosen for use in this project for a variety of reasons: they have viscoelastic properties at the extrusion temperatures that allow for multilayer co-extrusion with PSF, are in a rubbery equilibrium state at the temperatures of interest, have relatively low crystallinity compared to other options, and are not expected to interact favorably with PSF (*i.e.*, well-defined layers should be possible). Fig. 2 shows the second heating DSC

Table 1
Bulk material properties.

Polymer	Density	T_g	T_m	X_c	Tensile modulus	P_{O_2}	P_{N_2}	α_{O_2/N_2}
Polysulfone 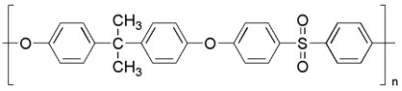	1.24	184 °C	–	–	2690	1.5	0.28	5.4
Engage 8100 (EO) 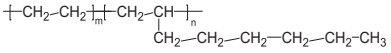	0.87	−52 °C	60 °C	15%	2.9	32	11	2.8
Infuse 9007 (OBC)	0.866	−60 °C	120 °C	8%	1.78	44	17	2.6

Density values taken from manufacturer data sheets; reported in units of g/cm^3.
Tensile modulus (ASTM D638) taken from manufacturer data sheets; reported in units of MPa.
Permeability values (at 35 °C) are reported in Barrers (Ba), where1 Ba $= 10^{-10}\,\frac{\text{cm}^3\text{(STP)cm}}{\text{cm}^2\text{s cmHg}}$.

thermograms of PSF, EO, and OBC scanned at 10 °C/min. By studying two different multilayered systems, the effect of the co-layering material on physical aging can begin to be addressed.

2.2. Multilayer co-extrusion

The films considered in this study were produced using a special co-extrusion system at Case Western Reserve University (CWRU). The details of the extruder setup and the production of multilayered films are described elsewhere [43,44]. A schematic illustration of the multilayer co-extrusion process is shown in Fig. 3. Two polymer melt streams are fed into a feedblock to produce the desired initial layer arrangement (ABA arrangement in this case). Special layer-multiplying dies then split, spread, and restack the stream so that the number of layers is essentially doubled with each successive die (ABABA…). At the end of the extruder, the exit die spreads the melt stream into a film roughly 30 cm in width where it is then taken up on a chill roll. The overall film thickness is controlled primarily by the total feed rate, while the layer thickness is dependent on the total feed rate, the number of multiplier dies, and the feed ratio of polymer A to polymer B.

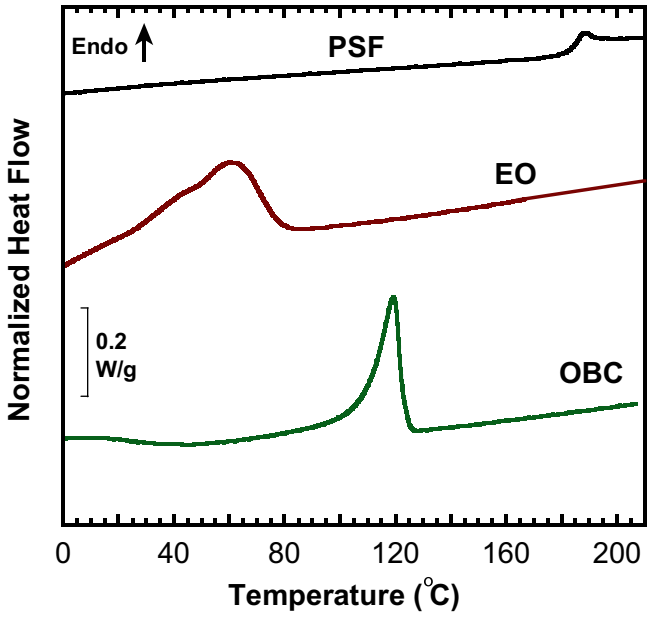

Fig. 2. DSC thermograms (2nd heat) of PSF, EO, and OBC scanned at a heating rate of 10 °C/min. The thermograms are normalized by the sample mass and offset vertically to permit easier viewing.

Table 2 contains information on the layered films studied, including the PSF content and layer thickness. The PSF/EO films, which were studied first, all have 257 layers and similar overall thickness but different PSF content, thereby producing films of different layer thicknesses. A sacrificial EO skin layer was added before the film exited the die, resulting in a layered PSF/EO film sandwiched between two thick EO layers. The thick EO layers were removed prior to aging studies, although removal was more difficult than expected based on the fact that PSF and EO should not strongly interact. The PSF/OBC films were produced by changing the number of layer multipliers and overall feed rate while holding the feed composition constant (50% PSF, 50% OBC), and no skin layer was applied to these films.

2.3. Characterization of multilayered films

Layer thickness was measured using atomic force microscopy (AFM). The average layer thickness was calculated from an AFM image by counting the number of layers in part of the sample, measuring the thickness of each individual layer, and then calculating the mean. The average layer thickness measured was typically within 10% of the target thickness calculated prior to the extrusion run. The standard deviation in layer thickness was typically 15–20% of the average value. AFM images confirm that the films are composed of continuous, well-formed layers (see Fig. 4 for a representative example). The overall thickness of the layered films was measured with a micrometer prior to permeation testing. A PerkinElmer DSC 6000 equipped with an Intercooler was used to characterize the thermal transitions in layered and bulk PSF films. DSC scans (second heating, 10 °C/min) of the layered films indicate that the T_g of the PSF layers, the T_m of the rubbery layers, and the crystallinity in the rubbery layers do not deviate from the bulk values. Scans for PSF/OBC films with different layer thicknesses are shown in Fig. 5 (a 129 layer film is included here but was not used in

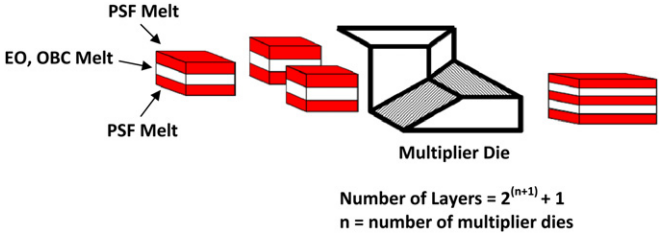

Fig. 3. Schematic illustration of co-extrusion scheme used to produce multilayered films [43].

Table 2
Composition and layer thickness data for layered films studied.

	Co-layering material	Nominal PSF content (vol. %)	Number of layers	Layer thickness	Overall thickness
1	EO	60%	257	400 nm	98 μm
2	EO	50%	257	320 nm	86 μm
3	EO	30%	257	190 nm	81 μm
4	OBC	50%	257	260 nm	126 μm
5	OBC	50%	513	185 nm	84 μm

gas permeation studies). It is evident from the thermograms that the melting points and glass transition temperatures do not appear to be affected by this type of layered confinement. Thus, any changes in aging behavior that may result from layered confinement are not due to changes in the T_g of the confined PSF material.

2.4. Gas permeability measurement

The permeability measurements reported here were made using a constant-volume, variable-pressure gas permeation cell described elsewhere [45]. All measurements were made at a temperature of 35 °C and an upstream pressure of 2 atm. During measurement, the downstream pressure never exceeded 10 Torr. Samples were stored at 35 °C in a desiccator box to prevent moisture absorption when they were not in the permeation cell for testing. In this study, the O_2 and N_2 permeability of each film was measured at various aging times up to ~2000 h.

Prior to beginning an aging study on a particular film, the film sample was annealed at 195 °C for ~15 min in a temperature-controlled oven, then removed and quenched to room temperature in air. Upon removal from the oven, the films pass through the PSF glass transition rapidly, reaching temperatures of at least 100 °C below T_g within 15 s and reaching room temperature within 30 s.

The temperature and annealing time were chosen so that the thermal history of the glassy layers could be well-defined while not causing the films to undergo layer breakup and phase separation.

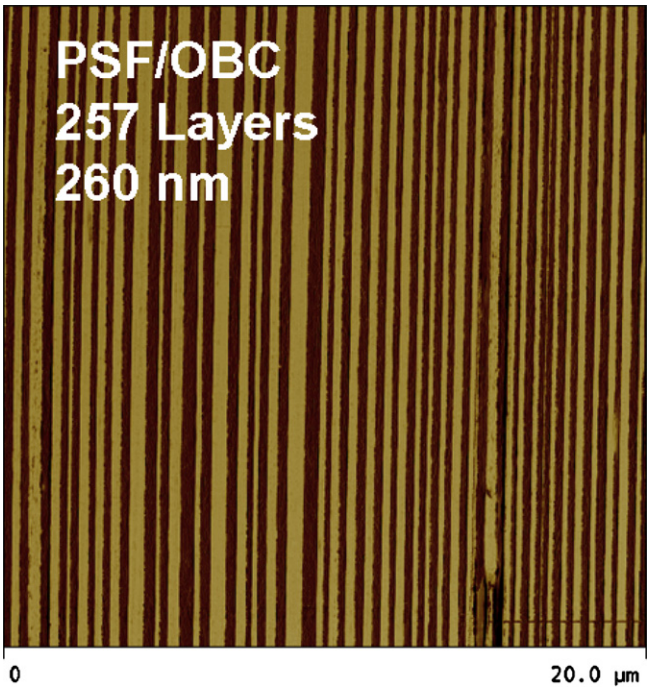

Fig. 4. AFM image of PSF/OBC layered film with 257 total layers and an average layer thickness of 260 nm.

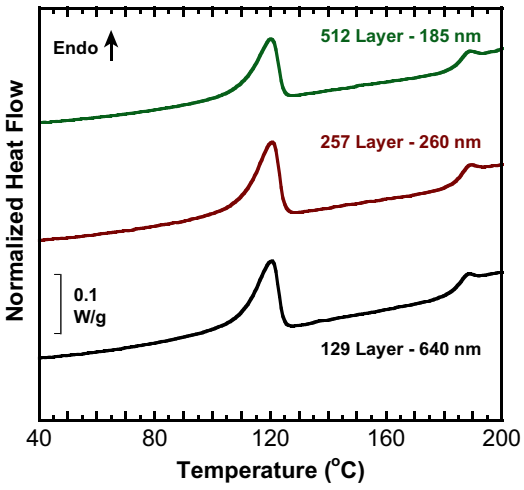

Fig. 5. DSC thermograms of layered PSF/OBC films. The thickness values given are those of the PSF layers, and the thermograms are normalized by the sample mass and offset vertically to permit easier viewing.

Visual inspection indicated that layer breakup did not occur, because the film remained partially transparent and did not become opaque and white (which was observed during experiments designed to produce layer breakup). Light transmission measurements and AFM images of annealed layered films confirmed that layer breakup does not occur under these annealing conditions. Annealing above T_g and then quench cooling ensures a reproducible thermal history and allows for a precise definition of the beginning of the aging study. The moment when the sample is removed from the annealing oven is defined as the "zero time", so the aging time simply represents the time elapsed since completing the annealing procedure.

3. Results and discussion

3.1. Permeability calculations

To facilitate comparison between films of different compositions, layer thicknesses, and overall thicknesses, it is useful to calculate the permeability of the PSF layers alone. This allows for a direct comparison between layered and bulk films, and it also enables comparison between the films considered in this study and the freestanding thin films studied by other researchers. The permeability of bulk EO and OBC films were measured at various times, and no changes in permeability with time were observed. Because the co-layering materials are well above their T_g values, the properties of those layers will not undergo changes due to physical aging (*e.g.*, McCaig measured the permeability of rubbery poly(-dimethylsiloxane) (PDMS) over time and did not observe any physical aging [16]). The series resistance model shown below was used to calculate the permeability of the PSF layers:

$$\frac{1}{P_{\text{layered}}} = \frac{\varphi_{\text{PSF}}}{P_{\text{PSF}}} + \frac{\varphi_X}{P_X} \tag{1}$$

In the above equation, the volume fractions of PSF and the co-layering material (EO or OBC) are represented by φ_{PSF} and φ_x, respectively; because the film is composed of only two polymers, φ_{PSF} and φ_x sum to unity. The PSF and co-layering material permeability values are represented by P_{PSF} and P_x, respectively, while the permeability of the composite layered film is P_{layered}. Knowing the volume fraction of PSF and the permeability of the co-

layering material enables calculation of the PSF layer permeability from measurements of the composite film permeability.

The calculation of layer permeability is subject to uncertainties in its inputs that affect the calculated result. For a film of PSF and EO with a nominal PSF volume fraction of 0.50, an uncertainty in the volume fraction of ±0.05 leads to uncertainty in the permeability value that is roughly ±10% of the value calculated using the nominal volume fraction (for films with lower PSF content, the effect on permeability is magnified). For example, the composite permeability of a 50/50 PSF/EO film is 2.7 Barrer (Ba), and the PSF layer permeability is calculated as 1.41 Ba using the nominal volume fraction of 0.5. If the film actually contains PSF at a volume fraction of 0.45, the calculated permeability should be 1.27 Ba; if the volume fraction were 0.55, the calculated permeability would be 1.54 Ba. Thus, uncertainties in the volume fraction can lead to noticeable over- or under-reporting of the proper absolute permeability value. Therefore, it is often useful to normalize permeability data to more easily compare the rate of permeability decline between different films, which may have significantly different absolute permeability values. The normalization procedure used here involves fitting a line to the linear portion of the calculated PSF layer permeability versus log(time) data, extrapolating the line back to an aging time of 1 h, and then using the permeability value at $t = 1$ h to normalize all other points in the data series. This procedure allows for straightforward comparison of the permeability decline and rate of aging and in bulk, multilayered, and thin films. Most of the discussion related to the figures presented here will focus on the PSF layer permeability and the normalized PSF layer permeability.

3.2. Gas permeability and aging in multilayered and bulk films

Figs. 6–8 present the time dependence of composite oxygen permeability for bulk PSF, PSF/EO, and PSF/OBC films, respectively. The results for the bulk "control" films of PSF produced during the PSF/EO and PSF/OBC extrusion runs are included in the respective plots for the multilayered systems. Fig. 6 allows direct comparison of the results for the two bulk films studied here with a film studied by Huang et al. [6]. While the two extruded films show nearly perfect agreement, demonstrating good reproducibility, the solution-cast film from Huang et al. shows a higher absolute permeability. The rate of permeability decline, however, appears similar in all bulk films. There are possible explanations for the differences in absolute permeability. The film studied by Huang et al. was prepared *via* solution casting, while the films studied here were produced *via* extrusion. McHattie et al. observed that sample preparation technique (*i.e.*, extrusion vs. solution casting) can significantly affect the measured permeability of PSF films, with extruded films always showing a lower permeability than cast films [46]. Additionally, the grade of PSF used in Huang's studies (Udel P-3500 NT LCD) is different from the grade used here (Udel P-3700), although many of the properties expected to affect permeability and aging behavior (*e.g.*, T_g and density) are the same for these two grades.

The composite permeability includes the contribution of the rubbery co-layering material, so the composite permeability values for the layered films are expected to be higher than bulk values. This expectation is borne out in Figs. 7 and 8. For our purposes, it is more relevant and interesting to consider the calculated PSF layer

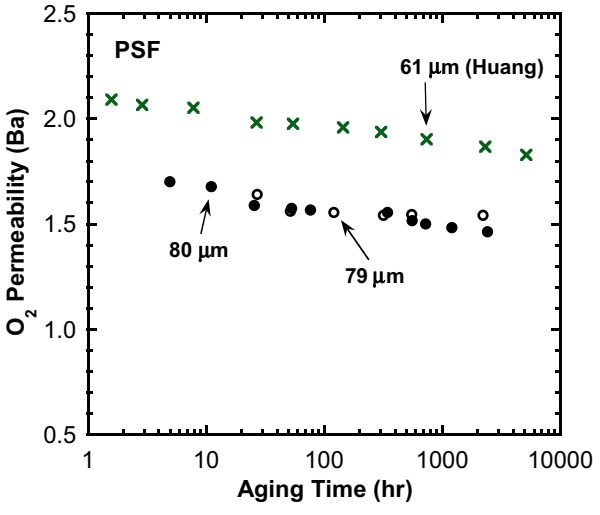

Fig. 6. Aging as monitored by oxygen permeability for thick (>50 µm) freestanding bulk PSF films at 35 °C. The data of Huang et al. are from the literature [6].

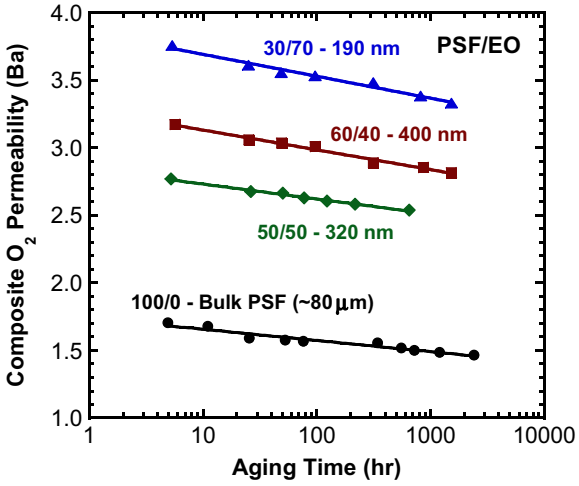

Fig. 7. Composite layered film oxygen permeability data for PSF/EO films aged at 35 °C. Data for bulk PSF film produced during PSF/EO extrusion run also included. All PSF/EO films contain 257 layers, and the thickness values given for layered films are those of the PSF layers. Lines are shown to guide the eye.

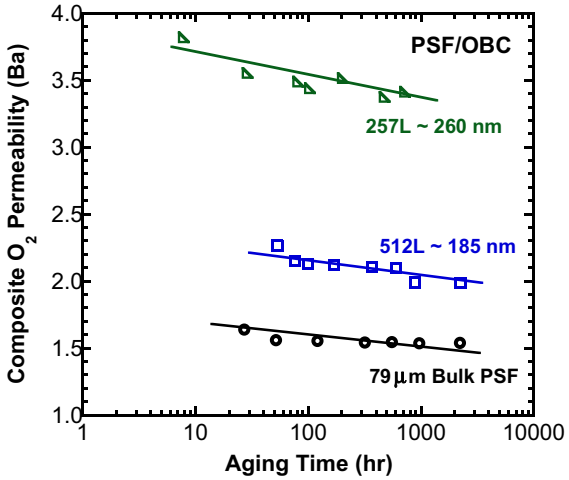

Fig. 8. Oxygen permeability of composite layered PSF/OBC films (257L = 257 layers; 512L = 512 layers). Data for bulk PSF film produced during PSF/OBC extrusion run also included. All PSF/OBC films have a nominal PSF content of 50% by volume, and the thickness values given for layered films are those of the PSF layers. Lines are shown to guide the eye.

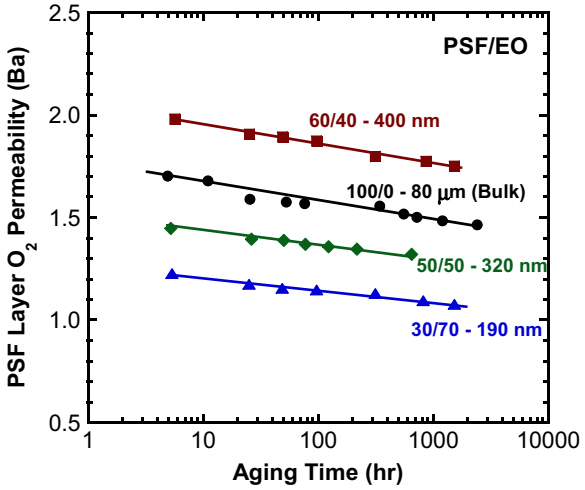

Fig. 9. Calculated PSF layer oxygen permeability data for PSF/EO layered films and bulk PSF film aged at 35 °C. Lines are shown to guide the eye.

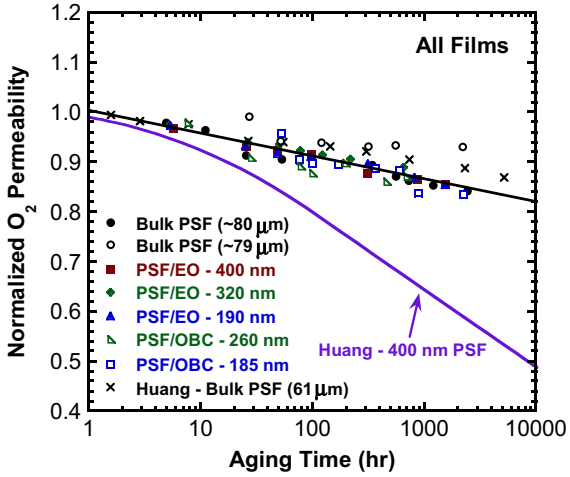

Fig. 11. Normalized oxygen permeability aging data for all films studied. Aging curves from Huang et al. [6] for a 400 nm freestanding PSF film and a 61 μm bulk film are taken from the literature and shown for comparison. The thickness values given for layered films are those of the PSF layers.

permeability determined using Eq. (1). Figs. 9 and 10 show the calculated PSF layer permeability for PSF/EO and PSF/OBC films, respectively. When examined individually, there appears to be a trend of higher permeability with increasing layer thickness for a given multilayered system (although the bulk permeability curves are below those for the most permeable layered film in both cases). When PSF/EO and PSF/OBC data are combined, however, this trend does not hold, so it is difficult to interpret the data any further. Additionally, the sensitivity of the calculated PSF layer permeability to the volume fraction of PSF (discussed in Section 3.1) suggests that some caution be exercised when interpreting the meaning of the absolute permeability values. Within a given figure (for Figs. 6–10), the decline in permeability appears to be similar for all films. Normalizing and then combining all the data makes it easier to compare the relative permeability decline in all the films considered.

Fig. 11 presents the normalized O_2 permeability data for PSF/EO, PSF/OBC, and bulk films, as well as a curve for a 400 nm PSF film studied by Huang et al. [6]. All bulk and layered film data essentially collapse onto a single line, indicating that the rate of permeability decline in all of these films is similar. The 400 nm PSF film (whose overall thickness is at the upper end of the range of layer thicknesses considered here) undergoes much more rapid aging than any of the bulk or multilayered films. At 1000 h of aging time, the 400 nm freestanding PSF film has decreased in permeability by 35%, whereas on average the bulk and multilayered films have only experienced a decline of 10–15%.

As polymer free volume decreases during physical aging, the permeability of larger gas molecules declines more rapidly than that of smaller ones [6]. Thus, the relative permeability decline of N_2 will be greater than that of O_2 (since N_2 is the larger molecule), and an increase in O_2/N_2 selectivity will be observed as the polymer ages. Fig. 12 shows the O_2/N_2 pure gas selectivity data for the films studied. As expected, the selectivity increases slightly as physical aging progresses for all films. The increase for the 400 nm freestanding thin film is slightly greater than that of bulk films, although the difference in the rate of selectivity increase is much less prominent than the differences in permeability decline observed for freestanding versus bulk films. The similarity in magnitude and rate of increase of selectivity in all films indicates

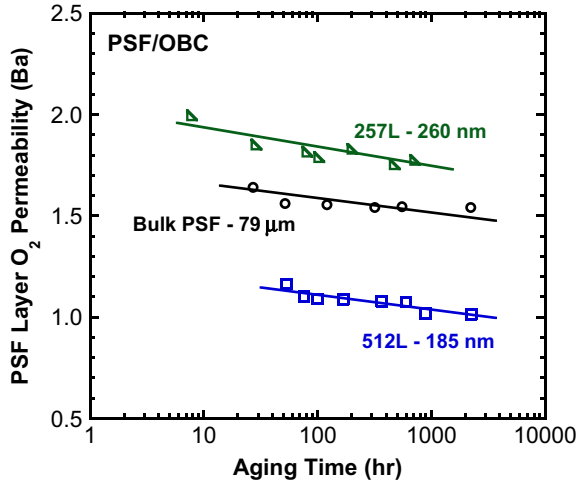

Fig. 10. Calculated PSF layer oxygen permeability for PSF/OBC films and bulk PSF film aged at 35 °C. Lines are shown to guide the eye.

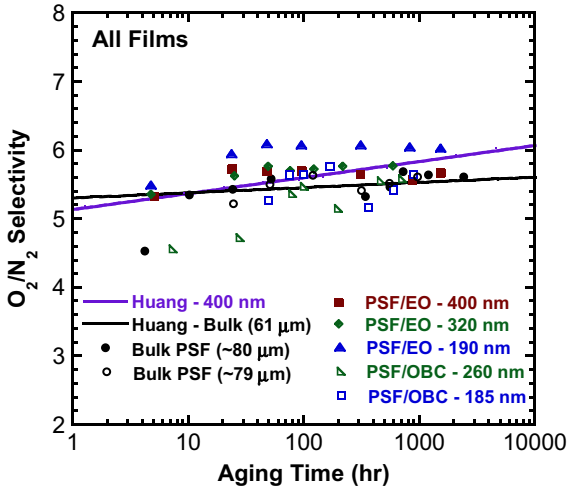

Fig. 12. Influence of physical aging on O_2/N_2 pure gas selectivity in PSF films. Solid lines are results from Huang et al. [6] for a 400 nm freestanding PSF film and a 61 μm bulk film. The thickness values given for layered films are those of the PSF layers.

that the N_2 permeability data should tell essentially the same story as the O_2 data. This is indeed the case, so plots of N_2 permeability are not shown for the sake of clarity and brevity.

Some potential reasons why the multilayered films age in a manner similar to bulk films can be identified. Enhanced mobility of polymer chains near free surfaces has been proposed as an explanation for decreased T_g and accelerated aging in thin polymer films [20,36,37]. It should be noted, however, that some studies of thin polymer films *via* dielectric spectroscopy do not observe significant changes in molecular mobility or T_g down to film thicknesses of 10 nm or less [47–49]. Sepúlveda et al. [50] studied aging in ultrathin films of toluene, a molecular glass former, and demonstrated that surface atoms are able to attain low-energy configurations more efficiently the those in the bulk, which leads to accelerated aging in thinner films. For thin, freestanding polymer films, a larger percentage of the sample is composed of near-surface material than for bulk films; thus, it is reasonable to expect a reduced T_g and a possible acceleration of physical aging in such films compared to bulk (depending on the aging temperature and the material's T_g). For the multilayered films studied here, there are many polymer–polymer interfaces ($2n$-2 for a film with PSF layers at the surfaces of the film, where n is the number of PSF layers) and few free surfaces (two), so the fraction of material near a free surface is more similar to that of a bulk film than a freestanding thin film. Thus, accelerated aging due to the enhanced free surface mobility associated with freestanding PSF films may not be observed in multilayered films.

The presence of the rubbery layers in these multilayered films could also impose a mechanical constraint on volume contraction that is absent in the case of freestanding films. In designing this study, relatively soft, low-modulus materials were chosen as co-layering materials for PSF to minimize this effect.

Another hypothesis that has been invoked to explain rapid aging in confined films is that free volume in the polymer can "diffuse" to free surfaces where it is then eliminated [11,16,17,51–53]. Because the timescale for diffusion is proportional to the square of the film thickness, thinner films would have smaller diffusive timescales and thus age more rapidly than thicker samples. In the layered films considered here, if the free volume cannot "diffuse" across the layer interface and be eliminated, the aging behavior observed would not be accelerated relative to bulk.

Another possibility is that during extrusion, which takes place at 290–300 °C, there are chemical reactions at the layer interfaces that introduce connectivity across the interface, thereby reducing the mobility of the near-interface polymer chains and leading to bulk-like aging behavior. One observation that lends credence to this notion is the fact that peeling the EO "skin layer" off of the PSF/EO films proved much more difficult than expected. In some cases, peeling the EO layer resulted in layer delamination and an uneven surface (only films with uniform surfaces were used for aging studies). It seems intuitively reasonable to suspect that chain connectivity across a layer interface would cause difficulty in removing the EO skin layer and could render the material near an interface less mobile than it would be otherwise. It should be noted that researchers using a PDMS coating technique to eliminate pinhole defects in glassy thin films found that the presence of a relatively thick PDMS layer on one surface of the thin film does not seem to change the aging behavior of the thin film within experimental uncertainty [20,54]. This technique involves spin-coating the PDMS atop the already-deposited thin film at room temperature and then curing it at temperatures below the T_g of the underlying glassy film. This experimental protocol should lead to well-defined PSF and PDMS layers with very little (if any) connectivity at the interface, which is one possible difference between the layered films discussed here and PDMS-coated thin films studied previously by others. Also, because the process of glass formation (which occurs upon removing a sample from the annealing oven and cooling through T_g) is different for freestanding and multilayered films, dissimilar aging behavior may be observed, as glassy materials are known to be highly history-dependent. Further investigation is required to pinpoint the reasons for bulk-like aging behavior observed in multilayered films and to determine whether other glassy materials behave similarly.

3.3. Aging rate comparison

A measure of aging rate, r_i, from permeability data can be defined as follows:

$$r_i = -\frac{\partial \log P_i}{\partial \log t} \tag{2}$$

where the subscript i refers to the gas species of interest. Fig. 13 presents the calculated aging rates from O_2 permeability data as function of layer or film thickness for thin (*i.e.*, ~400–4000 nm) and bulk PSF films studied by Huang et al. [6] and the bulk and layered films considered in this study. The aging rates in freestanding thin films show a strong dependence on thickness, and aging rates for each of these films, which range from roughly 0.05 to 0.1, are higher than for any bulk or multilayered film. The multilayered films do not show any noticeable dependence of aging rate on layer thickness, and aging rates in these films are essentially equal to those of bulk films. The aging rates for layered and bulk films are clustered around an average value of 0.02, implying that the films age in a similar manner. This result is significant, because it suggests that different types of confinement can affect property changes due to aging in different ways. There are potential benefits of having materials that are confined yet do not undergo rapid property changes. For example, some of the potential applications for extruded multilayered films involve optical applications where stability of relevant properties is important, such as gradient refractive index (GRIN) lenses [55] and polymer lasers [56].

3.4. Comparison to the permeability-selectivity upper bound

Polymeric membrane materials typically exhibit a tradeoff between permeability and selectivity, a concept first described

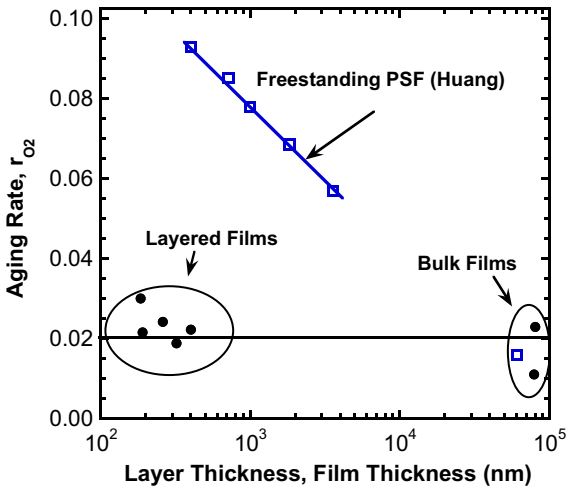

Fig. 13. Aging rates from oxygen permeability data for bulk, multilayered, and thin PSF films at 35 °C. Horizontal line shows average aging rate for all bulk and layered films. Data from Huang et al. [6] are given by the unfilled square symbols (□).

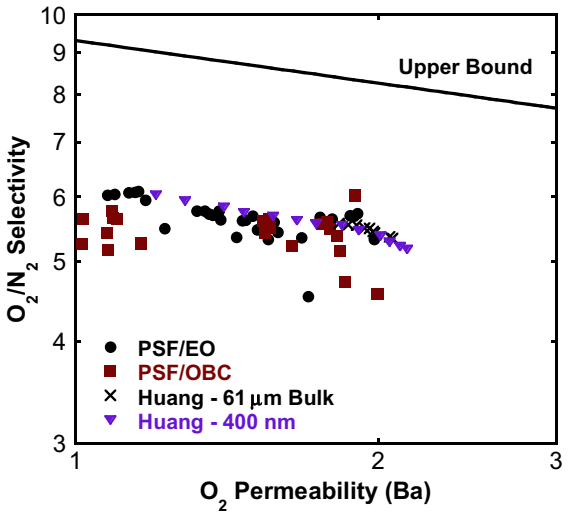

Fig. 14. Influence of physical aging on the tradeoff between permeability and selectivity and comparison with the upper bound [52]. Data from Huang et al. [6] are taken from the literature and shown for comparison.

empirically by Robeson as the "upper bound" [57,58]. The theoretical framework for upper bound behavior was developed years later by Freeman [59], and further study of the influence of temperature on the upper bound was recently published by Rowe et al. [60]. As a polymer undergoes physical aging, its permeability decreases while its selectivity increases. Fig. 14 is an upper bound plot for O_2 and N_2 containing data for PSF/EO and PSF/OBC layered films as well as for bulk and 400 nm PSF films studied by Huang et al. [6]. For all films shown, physical aging generally results in movement that is roughly parallel to the upper bound line. This trend is consistent with observations by Rowe et al., who found that PSF and Matrimid both experience property changes due to aging that cause movement parallel to the upper bound [20].

4. Conclusions

The physical aging of layered and bulk PSF films at 35 °C was studied by measuring gas permeability over time. These layered films age in a manner similar to that of bulk films, as demonstrated by the similarity amongst the rates of permeability decline for these two types of films. Freestanding thin films of PSF (*i.e.*, those studied by Huang et al. and Rowe et al., with overall thicknesses similar to the layer thicknesses of PSF/EO and PSF/OBC films) undergo more rapid aging than the films considered in this study. The thin PSF films studied by Huang et al. show a strong dependence of aging rate on film thickness, and the absolute magnitudes of the aging rates are higher for all thin films than they are for any bulk or layered film. Multilayered PSF/EO and PSF/OBC films show no dependence of aging rate on layer thickness, and the aging rates for the multilayered films are similar to those of bulk PSF films. In this study, the choice of confining polymer (EO or OBC) does not appear to affect the rate of aging. From this work, it appears that the effect of film thickness on physical aging stems from free surfaces and not merely thickness per se.

When plotted on an "upper bound" plot, permeability and selectivity changes due to aging cause movement parallel to the upper bound for bulk, multilayered, and freestanding thin films, which is consistent with past findings. The bulk-like aging behavior observed for multilayered films stands in sharp contrast to that of freestanding thin films, indicating that surfaces and interfaces play an important role during physical aging.

Acknowledgments

This research was supported by NSF Science and Technology Center for Layered Polymeric Systems (Grant DMR-0423914).

References

[1] Hutchinson JM. Progress in Polymer Science 1995;20(4):703–60.
[2] Struik LCE. Physical aging in amorphous polymers and other materials. Amsterdam: Elsevier; 1978.
[3] Hodge IM. Science 1995;267(5206):1945–7.
[4] Dorkenoo KD, Pfromm PH. Journal of Polymer Science Part B: Polymer Physics 1999;37(16):2239–51.
[5] Dorkenoo KD, Pfromm PH. Macromolecules 2000;33(10):3747–51.
[6] Huang Y, Paul DR. Polymer 2004;45(25):8377–93.
[7] Huang Y, Paul DR. Journal of Membrane Science 2004;244(1–2):167–78.
[8] Huang Y, Paul DR. Macromolecules 2005;38(24):10148–54.
[9] Huang Y, Paul DR. Journal of Polymer Science Part B: Polymer Physics 2007;45(12):1390–8.
[10] Huang Y, Paul DR. Industrial and Engineering Chemistry Research 2007;46(8):2342–7.
[11] Huang Y, Wang X, Paul DR. Journal of Membrane Science 2006;277(1–2):219–29.
[12] Kim JH, Koros WJ, Paul DR. Polymer 2006;47(9):3094–103.
[13] Kim JH, Koros WJ, Paul DR. Journal of Membrane Science 2006;282(1–2):21–31.
[14] Kim J, Koros W, Paul DR. Journal of Membrane Science 2006;282(1–2):32–43.
[15] McCaig MS, Paul DR. Polymer 1999;40(26):7209–25.
[16] McCaig MS, Paul DR. Polymer 2000;41(2):629–37.
[17] McCaig MS, Paul DR, Barlow JW. Polymer 2000;41(2):639–48.
[18] Pfromm PH, Koros WJ. Polymer 1995;36(12):2379–87.
[19] Rezac ME, Pfromm PH, Costello LM, Koros WJ. Industrial and Engineering Chemistry Research 1993;32(9):1921–6.
[20] Rowe BW, Freeman BD, Paul DR. Polymer 2009;50(23):5565–75.
[21] Rowe BW, Freeman BD, Paul DR. Polymer 2010;51(16):3784–92.
[22] Ellison CJ, Kim SD, Hall DB, Torkelson JM. The European Physical Journal E - Soft Matter 2002;8(2):155–66.
[23] Priestley RD. Journal of Physics: Condensed Matter 2007;19(20):205120.
[24] Priestley RD, Broadbelt LJ, Torkelson JM. Macromolecules 2005;38(3):654–7.
[25] Priestley RD, Ellison CJ, Broadbelt LJ, Torkelson JM. Science 2005;309(5733):456–9.
[26] Rittigstein P, Torkelson JM. Journal of Polymer Science Part B: Polymer Physics 2006;44(20):2935–43.
[27] Royal JS, Victor JG, Torkelson JM. Macromolecules 1992;25(2):729–34.
[28] Royal JS, Torkelson JM. Macromolecules 1990;23(14):3536–8.
[29] Royal JS, Torkelson JM. Macromolecules 1992;25(18):4792–6.
[30] Royal JS, Torkelson JM. Macromolecules 1993;26(20):5331–5.
[31] Baker EA, Rittigstein P, Torkelson JM, Roth CB. Journal of Polymer Science Part B: Polymer Physics 2009;47(24):2509–19.
[32] Huang Y, Paul DR. Macromolecules 2006;39(4):1554–9.
[33] Kawana S, Jones RAL. The European Physical Journal E - Soft Matter 2003;10(3):223–30.
[34] Kim JH, Koros WJ, Paul DR. Polymer 2006;47(9):3104–11.
[35] Pye JE, Rohald KA, Baker EA, Roth CB. Macromolecules 2010;43(19):8296–303.
[36] Kawana S, Jones RAL. Physical Review E 2001;63(2):21501.
[37] Rowe BW, Pas SJ, Hill AJ, Suzuki R, Freeman BD, Paul DR. Polymer 2009;50(25):6149–56.
[38] Ellison CJ, Torkelson JM. Nature Materials 2003;2(10):695–700.
[39] Forrest JA, Dalnoki-Veress K. Advances in Colloid and Interface Science 2001;94(1–3):167–95.
[40] Priestley RD. Soft Matter 2009;5(5):919–26.
[41] Koh YP, Simon SL. Journal of Polymer Science Part B: Polymer Physics 2008;46(24):2741–53.
[42] Boucher VM, Cangialosi D, Alegría A, Colmenero J, Pastoriza-Santos I, Liz-Marzan LM. Soft Matter 2011;7(7):3607.
[43] Mueller CD, Nazarenko S, Ebeling T, Schuman TL, Hiltner A, Baer E. Polymer Engineering and Science 1997;37(2):355–62.
[44] Liu RYF, Bernal-Lara TE, Hiltner A, Baer E. Macromolecules 2004;37(18):6972–9.
[45] Koros WJ, Paul DR, Rocha AA. Journal of Polymer Science: Polymer Physics Edition 1976;14(4):687–702.
[46] McHattie JS, Koros WJ, Paul DR. Polymer 1991;32(5):840–50.
[47] Labahn D, Mix R, Schönhals A. Physical Review E 2009;79(1):1–9.
[48] Serghei A, Huth H, Schick C, Kremer F. Macromolecules 2008;41(10):3636–9.
[49] Tress M, Erber M, Mapesa EU, Huth H, Muller J, Serghei A, et al. Macromolecules 2010;43(23):9937–44.
[50] Sepúlveda A, Leon-Gutierrez E, Gonzalez-Silveira M, Rodríguez-Tinoco C, Clavaguera-Mora M, Rodríguez-Viejo J. Physical Review Letters 2011;107(2):1–4.
[51] Cangialosi D, Wübbenhorst M, Groenewold J, Mendes E, Picken SJ. Journal of Non-Crystalline Solids 2005;351(33–36):2605–10.

[52] Cangialosi D, Wübbenhorst M, Groenewold J, Mendes E, Schut H, Veen A van, et al. Physical Review B; 2004:70224213.
[53] Boucher VM, Cangialosi D, Alegría A, Colmenero J. Macromolecules 2010; 43(18):7594–603.
[54] Cui L, Qiu W, Paul DR, Koros WJ. Polymer 2011;52(15):3374–80.
[55] Jin Y, Tai H, Hiltner A, Baer E, Shirk JS. Journal of Applied Polymer Science 2007;103(3):1834–41.
[56] Singer KD, Kazmierczak T, Lott J, Song H, Wu Y, Andrews J, et al. Optics Express 2008;16(14):10358–63.
[57] Robeson LM. Journal of Membrane Science 1991;62(2):165–85.
[58] Robeson LM. Journal of Membrane Science 2008;320(1–2):390–400.
[59] Freeman BD. Macromolecules 1999;32(2):375–80.
[60] Rowe BW, Robeson LM, Freeman BD, Paul DR. Journal of Membrane Science 2010;360(1–2):58–69.